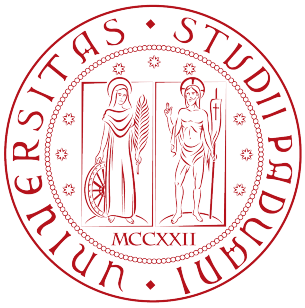

Università degli Studi di Universitá degli Studi di Padova

FACOLTÀ DI DIPARTIMENTO DI FISICA E ASTRONOMIA "GALILEO GALILEI"
Corso di Laurea Magistrale in Corso di Laurea Triennale in Fisica

Tesi di laurea triennale

Analysis of the diagnostic calorimeter measurements and characterisation of the particle beam of the BATMAN experiment

Candidato:
Massimiliano Ingrosso
Matricola 1008343

Relatore:
Dott. Gianluigi Serianni

Correlatore:
Dott.ssa Rita S. Delogu

Anno Accademico 2014–2015

Contents

Abstract

One of the main concerns of the modern world is energy production. As more non-renewable resources are expended, we need to research an alternative to fossil energy sources. ITER (International Thermonuclear Experimental Reactor) is one of the largest global project, that tackle this problem by nuclear fusion. Among the issues that need to be solved to achieve nuclear fusion, plasma heating is one of the most important.
One of the systems used for this scope is a Neutral Beam Injector (NBI). To study the beam characteristics, the test facility SPIDER is under construction in Padova. One of its diagnostics is the calorimeter STRIKE, whose main components are uni-directional CFC tiles. A prototype of the ion source, BATMAN, is operating at Max-Planck Institut für Plasmaphysik (IPP, Garching bei München, Germany) and is equipped with a prototype of the calorimeter, called mini-STRIKE.
The final objective is to reconstruct and characterize the energy flux impinging on a CFC tile in the BATMAN experiment. To this end, an inversion method was developed at Consorzio RFX, Padova, to obtain the two-dimensional profile of the energy flux from the corresponding temperature profile. The purpose of this thesis is to investigate the applicability and calibration of the inversion method, and subsequently to use it on experimental campaigns as a means to study the beam characteristics.
In Chapter 1, an overview of the energetic problem, nuclear fusion, plasma, ITER and a description of both the ion source and calorimeter are given.
Chapter 2 explains the main programs used in this thesis and gives an insight on the inversion method.
Chapter 3 shows the calibration procedure for the inversion methods, and the data analysis.
Finally, in Chapter 4 conclusions are presented.

Chapter 1

Introduction

The energy problem is one of the most discussed topics of the recent years, as humanity needs to find an alternative to fossil fuels before their depletion, and one of these alternatives that have been proposed is nuclear fusion.

1.1 Nuclear fusion

Nuclear fusion is one of the two methods in the atomic world to create a large amount of energy (the other being fission). A nucleus with enough velocity (energy) can penetrate the Coulomb barrier of another nucleus. In this case there are two forces that act in the process: the Coulomb force and the nuclear force. According to Figure 1.1, the best candidates for nuclear fusion reaction are deuterium and tritium nuclei. The equation 1.1 summarizes the process:

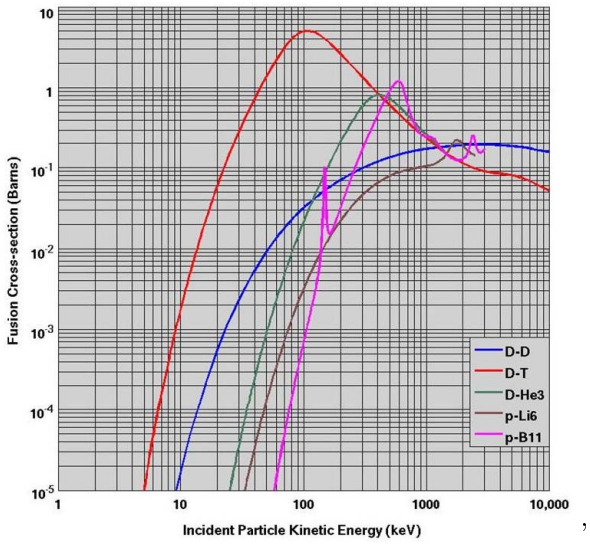

Figure 1.1: Cross sections of fusion reaction of species candidates for ITER[2]

$$^2\mathrm{D} + {}^3\mathrm{T} \rightarrow {}^4\mathrm{He} + \mathrm{n} \tag{1.1}$$

To overcome the Coulomb barrier and have a nuclear fusion reaction, particles need to have sufficient kinetic energy. To achieve this end plasma is used.

1.1.1 Plasma

Plasma is defined as a gas with these properties:

- has some degree of ionization
- quasi-neutrality of the gas $n_e \approx n_i \approx n$[1]
- has a collective behavior

Additionally, when a charged particle is introduced inside the plasma, it is shielded from the rest of the plasma, as particles are free to move when subjected to electric potential: ions and electrons will misplace themselves in order to counter the the electric field of the new charged particle. In this case, Debye lenght is defined as the length where near particles can be affected by the introduced charge, since the shielding reduce the electrostatic potential:

$$\lambda_D = \left(\frac{\epsilon_0 k_b T_e}{ne^2}\right)^{\frac{1}{2}}{}^2. \tag{1.2}$$

Another important parameter of the plasma is the electron frequency, the frequency of electrostatic oscillation caused by a small charge separation:

$$\omega_e = \left(\frac{ne^2}{\epsilon_0 m_e}\right)^{\frac{1}{2}}{}^3. \tag{1.3}$$

1.1.2 Boundary conditions of the nuclear fusion

To achieve the desired reaction, there are some physical conditions that need to be met. Particularly, the Lawson criterion sets a threshold:

$$n\tau_E \geq \frac{12 k_b T}{E_\alpha \langle v\sigma \rangle} \tag{1.4}$$

where n is the plasma (numerical) density, τ_E the energy confinement time[4], T is the plasma temperature, E_α is the energy of the ^{4}He released in the fusion reaction, and $\langle v\sigma \rangle$ is the reaction rate coefficient. The optimal values needed for the fusion reaction 1.1 are a temperature of 15 keV and a plasma density of 10^{20} m^{-3}.

Two main issues are important when trying to achieve nuclear fusion:

[1] n_e and n_i are respectively the numerical density of electrons and ions

[2] ϵ_0 is the permettivity of free space, k_b is the Boltzmann constant, T_e is the electron temperature, n is the density of plasma, e is the elementary charge

[3] m_e is the electron mass

[4] energy confinement time is defined as $\tau_E = \frac{W}{P - \frac{\mathrm{d}W}{\mathrm{d}t}}$ [3]

- Plasma heating
- Plasma confinement

Concerning the latter two kinds of confinement methods seem to be the most promising:

- Inertial Confinement
- Magnetic Confinement

The most important nuclear fusion project, ITER (International Thermonuclear Fusion Reactor, see figure 1.2) a tokamak machine, will be focused on magnetic confinement. The plasma heating system will be discussed later in this work.

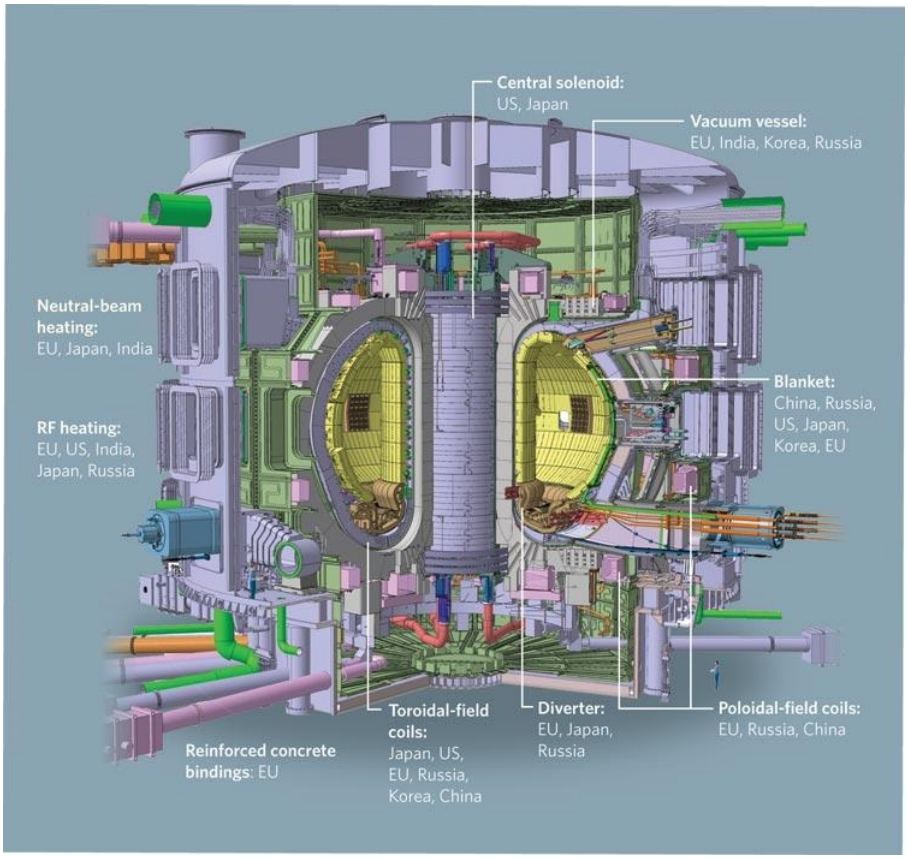

Figure 1.2: Model of ITER fusion reactor[1]

1.1.3 Tokamak fusion reactor

Tokamaks[5] belong to the group of magnetic confinement where, as the russian name indicates, magnetic fields are used for confining hot plasmas in a steady-state configuration. Of the two approaches, magnetic confinement is more developed and is considered to be the first to lead to a fusion reactor. In the first years of fusion research on magnetic confinement, many magnetic schemes were investigated, from toroidal systems such as tokamaks, stellarators, reversed field pinches, to open systems such as mirrors and cusps. It became clear that tokamaks were by far the most successful and had the best chance of leading to a fusion reactor. This is why the tokamak configuration was chosen for ITER). Inside a tokamak the plasma is confined by a strong toroidal magnetic field (B_T), which is produced by external coils (toroidal magnets), together with the poloidal field (B_P) produced by a toroidal current flowing in the plasma and by external coils[5]. A diagram of the tokamak can be seen in figure 1.3.

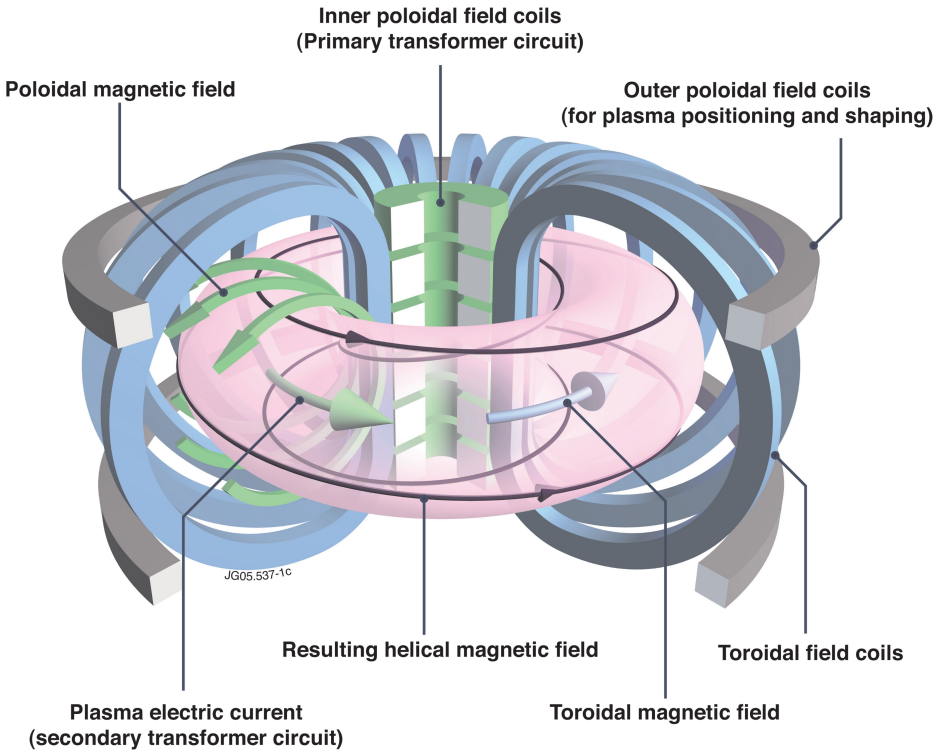

Figure 1.3: Scheme of the magnetic fields inside a Tokamak[6]

[5]a tokamak is a device that uses magnetic confinement for plasma, studied in Russia after the Second World War by I.E. Tamm, A.D. Sakharov and other scientists[4]

1.2 Plasma Heating

In the ITER experiment, three ways are used to heat plasma:

- Ohmic Heating
- Radiofrequency Waves (RF)
- Neutral Beam Injector (NBI)

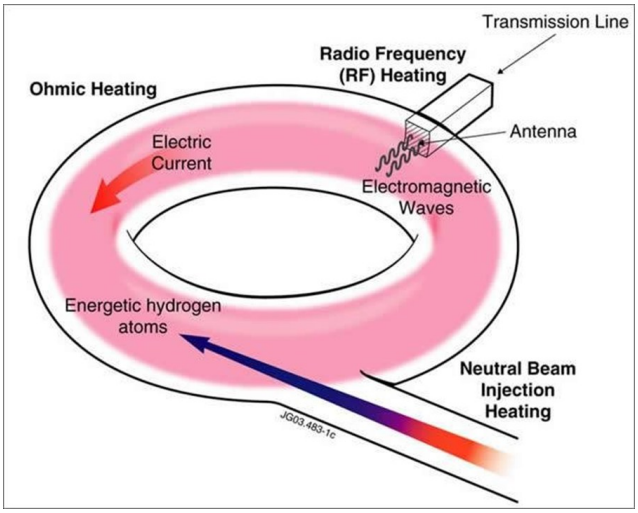

Figure 1.4: Plasma heating overview

In the first one a toroidal current, driven along the torus, heats the plasma according to the ohmic law $P = R \cdot I_p$, where R is the plasma ohmic resistance, I_p is the current and P the power deposition. The current in the plasma is induced by the variation in time of the poloidal magnetic field generated by an external coil located at the center of the torus. Since R is inversely proportional to the temperature of the plasma, the Ohmic heating efficiency decreases along the process, leading to a maximum achievable temperature far lower than the required temperature[7]. So, ohmic heating can be used to heat cold plasma, but further heating requires additional methods.
For the second method, high frequency electromagnetic waves are injected into the plasma. Different components and locations of the plasma itself are heated according to the frequency range involved. The typical frequencies belong to the range of the low frequency Alfven waves ($1 \div 10$ MHz), ion cyclotron frequencies ($30 \div 100$ MHz), lower hybrid frequencies ($1 \div 10$ GHz) and electron cyclotron frequencies ($50 \div 150$ GHz).
Regarding the neutral beam injector, negative or positive ions are accelerated at very high energies (50 kV $\div$1 MV), and neutralized; then they can penetrate the magnetic field. Colliding with electrons and ions the particles are finally ionized and trapped. They will transfer their kinetic energy to the plasma by collisions, thereby heating the plasma. Negative ion source will be used in ITER

neutral beam injectors since the required energy of the beam injected is 1 MeV, a result unachievable with a positive ion source, as the neutralization efficiency of positive ions drops to unacceptable level (figure 1.5) at the desired energy. The prototype of the neutral beam injector that will be used for ITER is MITICA (Megavolt ITER Injector and Concept Advancement), under construction in Padova. To solve physical and technological issues (see table 1.1 for ITER requirements) a prototype of the ion source equal in dimension, SPIDER (Source for the Production of Ions of Deuterium Extracted from an RF plasma), is also under construction at Padova. Before SPIDER is completed, another test facility has been built and tested at IPP-GARCHING, the device BATMAN (Bavarian test machine for negative ions) that has the objective of optimising the source performance

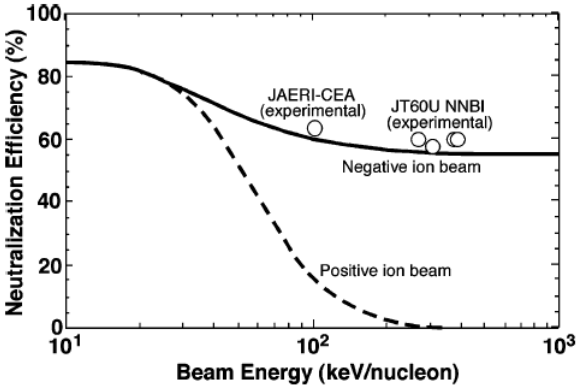

Figure 1.5: Neutralisation Efficiency Comparison [8]

Table 1.1: Required Performance of the ITER Negative Ion Source in deuterium

Source dimensions	1.9×0.9 m^2
Beam Energy	1 MeV
Negative ion current (current density)	40 A ($330 A/m^2$)
Ion extraction area	576 mm $\times$ 1534 mm
Operating pressure	< 0.3 Pa
Co-extracted electron current ($^{I_e}/_{I_{D^-}}$)	≤ 1
Pulse duration	3600 s
Beam energy	≤ 7 mrad

1.3 Structure of a Neutral Beam Injector

A NBI consists of four parts: the ion source, the accelerator system where the ion beam is formed, the cell where ions are neutralized and the residual ion

dump that with a magnetic or electrostatic field deflects and removes unwanted ions from the beam.

1.3.1 Ion Source

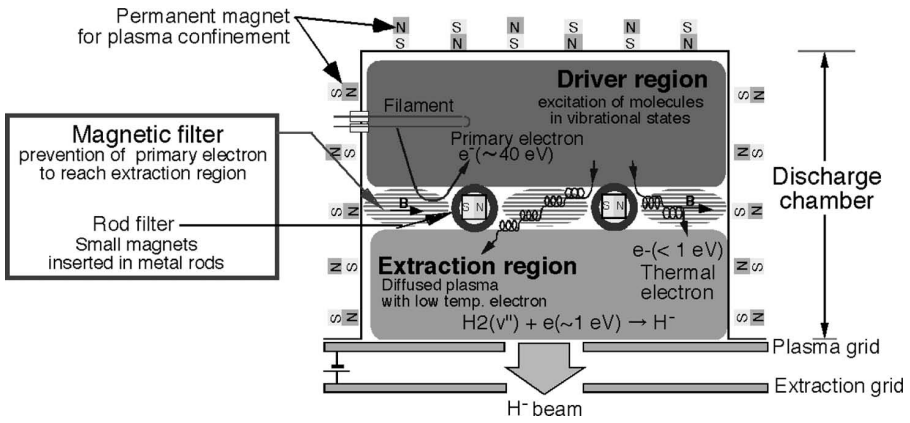

Figure 1.6: NBI Source with arc filament as driver[8]

A scheme of the ion source is illustrated in figure 1.6. To ionize the gas inside the ion source and generate the plasma, a device is needed to couple energy to particles. An arc filament was tested first. However, sputtering[6] reduces the filament lifetime to unacceptable levels and deteriorates the operation of the negative ion source, and so another option was tested, a RF coil. Inside the ion source a RF coil induces an oscillating electric field that accelerates free electrons(figure 1.6), thus ionizing the gas inside the ion source and then generating plasma.
A series of permanent magnets, located outside the ion source wall, shapes a magnetic field to contain plasma. The ion source is divided in the driver region and the expansion region by the magnetic filters. These are installed to manipulate the flow of electrons: they create a magnetic field that deviates energetic electrons back in the driver region, while cold electrons diffuse in the expansion region. The ions will be then extracted by means of a series of grids that will be described in the next sections. Creations of ions can occur via volume or surface processes.

Volume processes

The volume processes are due to dissociative attachment of electrons to highly vibrationally excited hydrogen molecules in their electronic ground state:

$$\mathrm{H}_2 + e_{\mathrm{fast}} \rightarrow \mathrm{H}_2^*(v) + e$$
$$\mathrm{H}_2^*(v) + e_{\mathrm{slow}}{}^7 \rightarrow \mathrm{H}^- + \mathrm{H}^0$$

[6]Sputtering is a process whereby particles are ejected from a solid target material due to bombardment of the target by energetic particles[9].

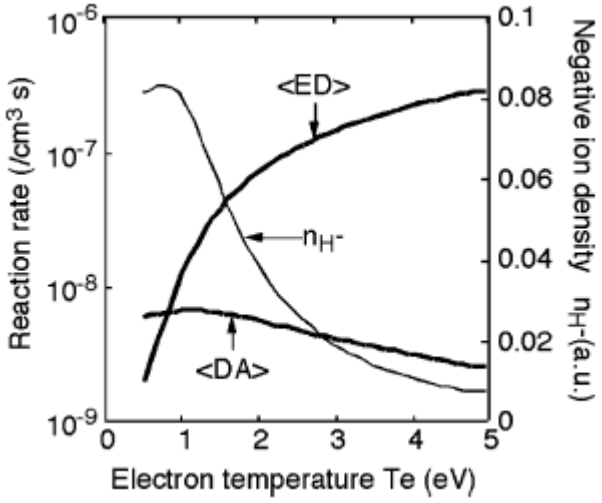

Figure 1.7: Reaction rates of the processes as functions of electronic temperature[8]

Destruction volume processes have to be taken into account as well. There are three major ones: electron detachment (ED), mutual neutralization (MN) and associative detachment (AD)

$$\begin{aligned} \text{ED: } & \mathrm{H}^- + e \rightarrow \mathrm{H}^0 + 2e \\ \text{MN: } & \mathrm{H}^- + \mathrm{H}^+ \rightarrow 2\mathrm{H}^0 \\ \text{AD: } & \mathrm{H}^- + \mathrm{H}^0 \rightarrow \mathrm{H}_2 + e \end{aligned}$$

with an electronic temperature of $1eV$, the two major processes are dissociative attachment and electron detachment. The negative ion density is then given by

$$n_{\mathrm{H}^-} \approx \frac{n_{\mathrm{H}_2^*\langle\ \mathrm{DA}\ \rangle}}{\langle\ \mathrm{ED}\ \rangle} \tag{1.5}$$

$\langle$ ED $\rangle$ and $\langle$ DA $\rangle$ are the reaction rates of the respective processes.

While there is a weak relationship between $\langle$ DA $\rangle$ and electronic temperature, ED instead rises quickly in comparison in the same temperature range ($1-2$ eV, as shown in figure 1.7), so a low temperature of electrons is necessary to have a high ion density. Magnetic filters take care of this aspect, as already described.

[7] v is the vibrational state level, $\mathrm{H}_2^*(v)$ is the vibrationally excited hydrogen molecule

Surface processes

Hydrogen interacts with surfaces producing negative ions according to the reaction:

$$H + e^-_{surface} \rightarrow H^-, H^+ + e^-_{surface} \rightarrow H^-$$

To maximise the amount of negative hydrogen atoms, a thin and homogeneous cesium layer covers the first grid of the extraction system, in order to reduce the work function[8] to approximately 2 eV [17]. The survival length of the negative ions in the source plasma is in the order of a few centimeters [18], so only ions created in the vicinity of the plasma grid can be extracted. As the electrons in this region have a lower temperature, the mean free path of negative hydrogen ions increases to few tens of centimeters.

Extraction region

The extraction and acceleration system used for BATMAN, SPIDER and MITICA is a grid system. In the case of BATMAN there are three grids and a plate:

- bias plate BP
- plasma grid PG
- extraction grid EG
- grounded grid GG

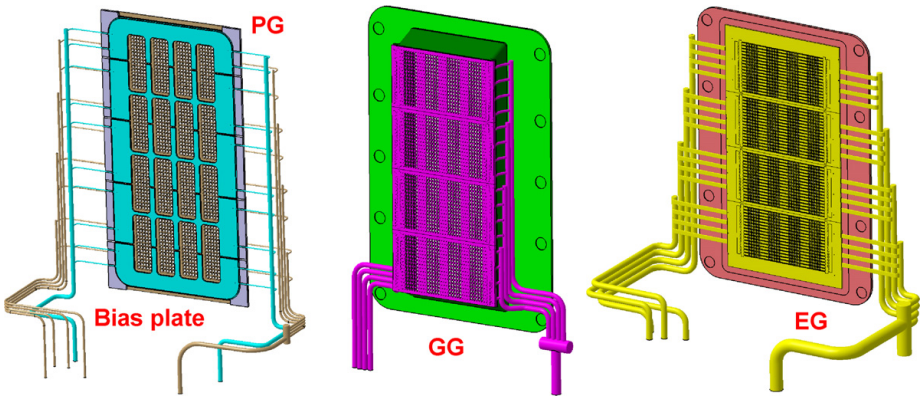

Figure 1.8: Models of the grid system for MITICA[14]

every grid has many apertures, through which ions are extracted from the source. Ions passing through the grid opening are accelerated by means of electric voltage and form a beamlet. All the beamlets toghether form the beam.

[8] the work function is the minimum thermodynamic work necessary to remove an electron from a solid into the vacuum outside the surface of the solid. It is defined by $W = -e\phi - E_F$, where e is the elementary charge, ϕ is the electrostatic potential of the vacuum and E_F is the Fermi level inside the material[16].

The bias plate is at potential of the source walls and the plasma grid is biased positively with respect to the ion source body. The bias plate is added to the system in order to reduce the amount of co-extracted electrons (as a side effect also the amount of extracted negative ions is reduced [8]).
The boundary between source potential and extraction potential is called meniscus, and it is defined as the surface where the potential is zero with respect to the source. The extraction grid is equipped with magnet rods that deviate co-extracted electrons on it. The co-extracted electrons are deflected onto the extraction grid and transfer kinetic energy. One of the limits that a NBI has is this power over the extraction grid; to minimize this effect, the ratio between co-extracted electrons and ions can be at maximum 1. Also the ions are affected by the magnetic field, even if in a smaller scale ($\frac{m_e}{m_{H^-}} \ll 1$). The potential between plasma grid and extraction grid is called "extraction potential". The grounded grid is set at zero potential, and the potential between it and the extraction grid is the "acceleration potential". Usual values of the various voltages are shown on table 1.2. An important phenomenon inside the accelerator is stripping, the neutralization of H^- inside the grid. If a particle is neutralized inside the grid system, it will no longer be accelerated by the potentials, thus lowering the energy flux. Since stripping is a function of the pressure, to minimize this phenomenon the pressure must be low (≤ 0.3 Pa).

Table 1.2: Batman Grid Data

Bias Voltage	$10 - 20$ V
Extraction Voltage U_{ext}	$5 - 10$ kV
Acceleration Voltage U_{acc}	$8 - 15$ kV
Electronic power deposited on extraction grid	25 kW

1.3.2 Drift region

In the drift region, negative ions that have been accelerated, are neutralized (60% of the total). Then, the ions not neutralized are deviated by means of electrostatic or magnetic field. Those ions are collected by the residual ion dump. Finally, the neutral beam is injected into the plasma.

1.4 STRIKE

STRIKE (see figure 1.11) stands for Short-Time Retractable Instrumented Kalorimeter[10], it is the instrument by which the beam of SPIDER will be characterized. Mini-STRIKE is its prototype, used in BATMAN[11] experiment, to test the capabilities of such device and optimizing it. The main component of both system are one-directional carbon fibre carbon composite tiles. STRIKE features 16 tiles, as many as SPIDER beamlet groups (4×4); the tiles are hit by the beam, and a thermal camera observes the tiles: a temperature profile is acquired. Analysis on the thermal profile provides information about the energy flux on the front side.
Mini-STRIKE features two tiles that are located about 1 m from the grounded

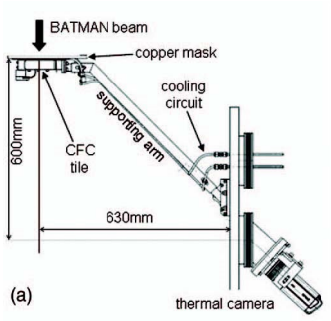

Figure 1.9: Sketch of mini-STRIKE[19]

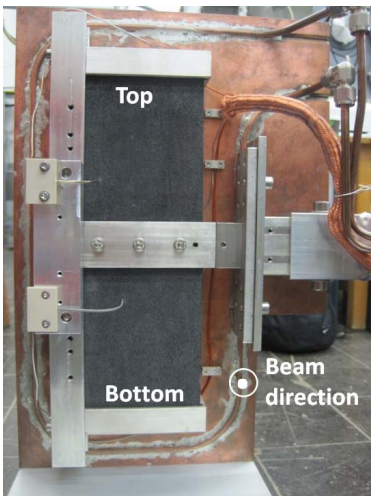

Figure 1.10: Rear side of mini-STRIKE

grid and are perpendicular to the beam direction. In BATMAN the divergence of the beamlets is larger than 1° and so at the CFC tiles they overlap. An actively cooled copper mask is placed in front of the CFC tile in order to create an artificial beamlet-like structure on the tiles. The copper mask has 18×2 holes (one set per tile) of 7 mm diameter. After passing through the copper mask, the surviving BATMAN beam reaches the front side of the CFC tile, and the kinetic energy is transfered to it and a temperature profile can be observed on the backside. Two thermocouples are placed on the backside to measure the temperature of each tile as a comparison for the thermographic measurement. The infrared camera mounted on mini-STRIKE observes the area of the CFC tiles from the back-side. We can't directly observe the energy flux because the acquire images would be distorted by beam interactions with background gas and the CFC tiles dust. Pulses last for 3 or 4 seconds and the background is evaluated a couple of seconds before the start. The camera is at a viewing angle of 50°, it acquires 25 frames per second, for a total of 500 frames in total. Each frame is a 640 $\times$ 480 matrix of pixels,. The error associated with the temperature measurements is 2 K or 2%, whichever is the higher. The camera is activated 3.2 s before the pulse starts as a comparison for the thermographic measurement. The main characteristic of the CFC tile is its strong anisotropic thermal conductivity[12]. Along the z-axis there is a thermal conductivity 25 times higher than the ones along the x-axis and y-axis. This means that the temperature profile will be similar to the energy flux one.

Table 1.3: mini-STRIKE CFC tile specification[12]

Spatial Dimensions	$120 \times 90 \times 20$ mm^3
Distance from GG	≈ 1 m
Emissivity	$\epsilon \approx 1$
Specific heat	$c_s = 767$ J/kg·K
Density	1950 kg/m^3
Thermal Conductivity (at 293.15 K)	κ_x,$\kappa_y \approx 20$ W/m·K, $\kappa_z \approx 550$ W/m·K

Table 1.4: Thermal Camera Specifications

Acquisition Frequency	$25 \frac{\text{frames}}{s}$
Image dimensions	640×480 pixels

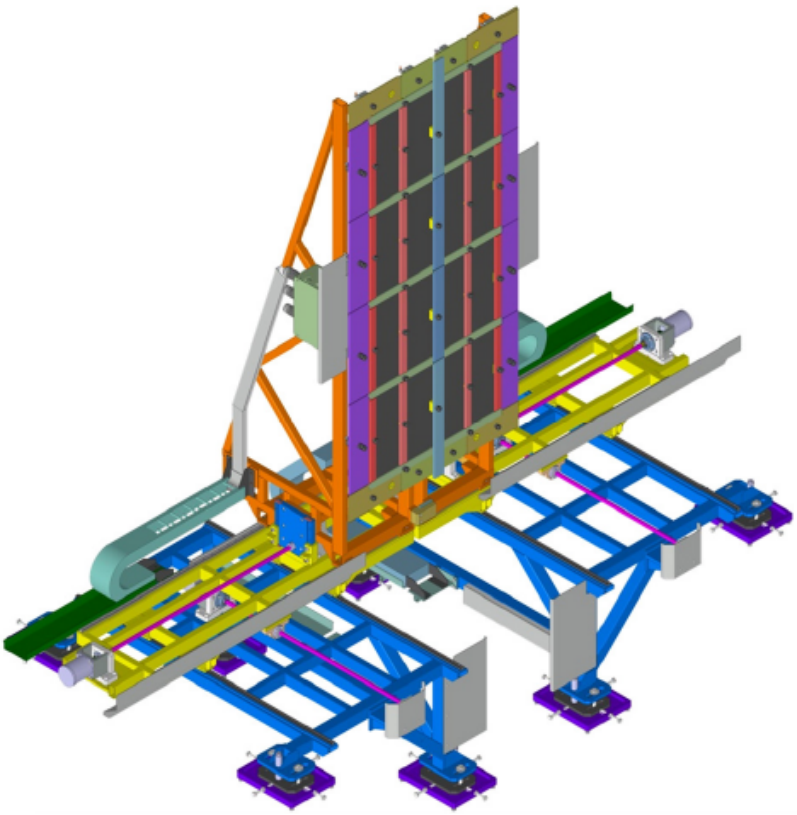

Figure 1.11: STRIKE model, closed [20]

1.5 Perveance

In the case of beam optics, space charge of the beam influence the beam itself. Perveance indicates the effect of the space charge on beam motion, and particularly on beam divergence. Perveance is defined as

$$P = \frac{\mathrm{I_{ex}}}{\mathrm{U_{ex}^{\frac{3}{2}}}}, \tag{1.6}$$

where $\mathrm{I_{ex}}$ is the extracted current and $\mathrm{U_{ex}}$ is the extraction voltage. The maximum perveance can be defined as well, deduced from the maximum possible extractable current, given from Child-Langmuir law[15]:

$$I_{ex}^{max} = \frac{4}{9}\pi\epsilon_0\sqrt{\frac{2e}{m}}\frac{r^2}{d^2}\mathrm{U_{ex}^{\frac{3}{2}}} \tag{1.7}$$

where ϵ_0 is the free space permittivity, e is the electron charge, m is the mass of the particle, r is the radius of the apertures of the grid system and d is the distance between plasma grid and extraction grid.

and thus Π_0 is

$$\Pi_0 = \frac{4}{9}\pi\epsilon_0\sqrt{\frac{2e}{m}}\frac{r^2}{d^2}. \tag{1.8}$$

This parameter is most important to evaluate the beam optics. The beam optics is determined by the beamlet optics, in particular the most noteworthy value is its divergence, as MITICA requires a beam divergence $\epsilon \leq 7$ mrads. Beamlet divergence is function of the normalized perveance and the ratio of extracted voltage to acceleration voltage. There is a local minimum of the divergence as a function of the normalised perveance between 0.1 and 0.2, which is the optimum perveance : the region before the minimum is called under-perveant region, and the region after the local minimum is called over-perveant region. In the case of the under-perveant region, the electric field is not strong enough to compensate for the beamlets expansions, while in the over-perveant region the opposite case takes place; in any case, the result is an increased divergence.

Chapter 2

Software used for data analysis

Three different programs has been used for the analysis of the data: the inversion program (based on Matlab), the fit program (based on IDL) and the transfer program (based on COMSOL Multiphysics).

2.1 Inversion program

With the current instrumentation a direct observation of the energy beam is impossible, or at least quite difficult. The only profile that can be observed "directly" is the temperature one. To have an approximation of what the energy flux is the inversion method was conceived. The inversion program analyzes a pixels matrix that has been manipulated from the image acquired by the thermal camera. After removing the background and recovered the perspective, the area of the tiles is selected (see figures 2.1, 2.2 and 2.3)

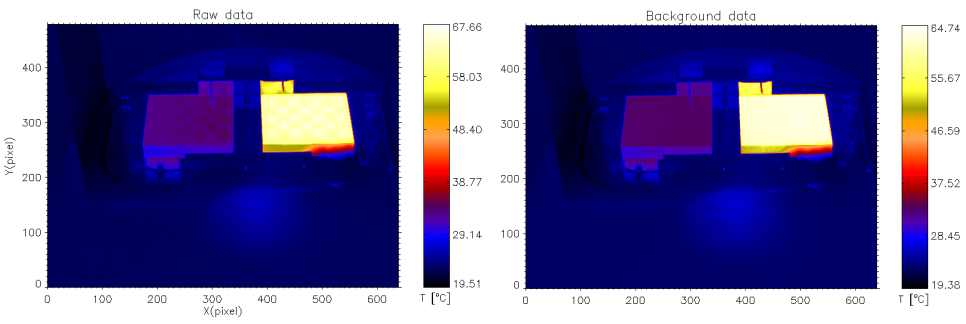

Figure 2.1: Raw data image and background used for subtraction

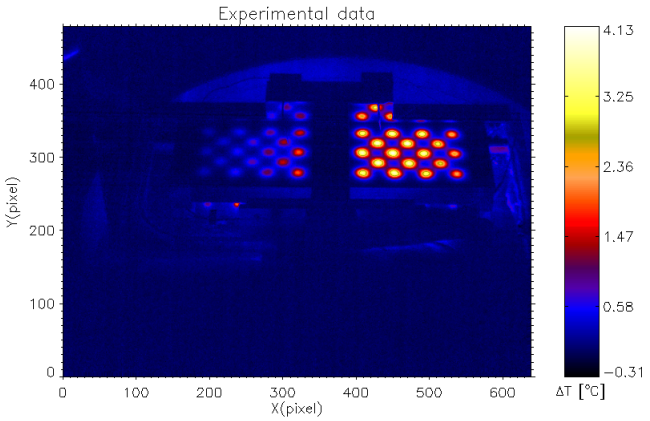

Figure 2.2: Experimental data image

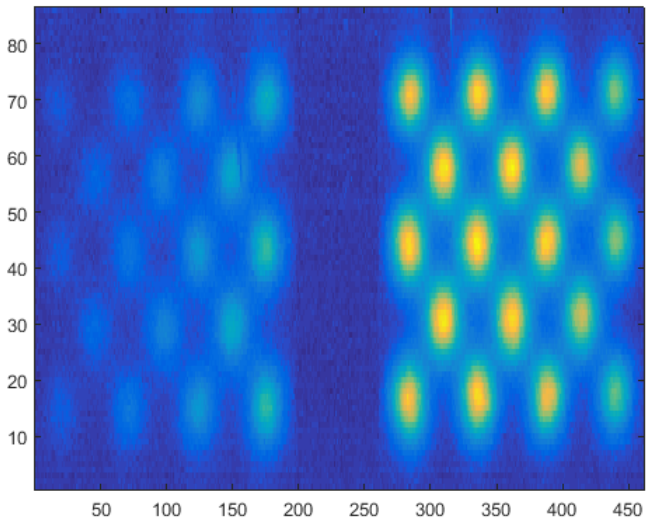

Figure 2.3: Data image with cut and perspective correction

2.1.1 Transfer function

As already mentioned in the precedent section, both STRIKE and mini-STRIKE feature a CFC tile on which the neutral beam hits the front side. We can sketch this process as a system that given an input (the energy flux profile) produces an output (the temperature profile) by the means of a transfer function. We can use the anti-transfer function to re-construct the flux from a temperature profile[21].

The used to represent for the temperature profile is a two dimensional Hubbert function

$$\overset{\text{energy flux}}{u_t^\delta} \Longrightarrow U_t^\delta \Longrightarrow \overset{\text{CFC tile}}{\boxed{F_t(k,j)}} \Longrightarrow V_t^\delta \Longrightarrow \overset{\text{temperature}}{v_t^\delta}$$

Figure 2.4: Sketch of the process

$$v_t^\delta = A_v \left(\cosh \sqrt{(x-x_c)^2 b^2 + (y-y_c)^2 d^2}\right)^{-\gamma} \tag{2.1}$$

where x_c and y_c describes the position of the peaks, b and d are the inverse of the HWHM parameter of the curve (this representation is to ease computational cost to the program). The function that is assumed to represent the energy flux profile is a two dimensional Gauss function:

$$u_t^\delta = A_u \exp\left(-\frac{1}{2}\left(\left(\frac{x-x_c}{\sigma_x}\right)^2 + \left(\frac{y-y_c}{\sigma_y}\right)^2\right)\right). \tag{2.2}$$

Given the Fourier transforms $U_t^\delta(k,j)$ and $V_t^\delta(k,j)$, respectively U the bi-dimensional Fourier transform of the point-like energy flux at time t and V the bi-dimensional Fourier transform of the temperature at time t , the anti-transfer function is:

$$G_t(k,j) = \frac{U_t^\delta(k,j)}{V_t^\delta(k,j)}. \tag{2.3}$$

The 2.3 is valid under the following boundary conditions:

- The CFC tile has a negligible black-body radiation
- negligible signal transfer delay from front side to rear side, with respect to the frame rate of the thermal camera.

The energy flux is then obtained by the convolution $G * v$[1].

The temperatures profile (Hubbert function) is smoother and broader than the energy flux, but this relationship is reversed in Fourier space. The anti-transfer function acts as a high pass filter and so there can be oscillation phenomenas that are exalted by it. To take into account this effect this effect, a low-pass filter[2] has been deployed.

2.2 Fit program

The fit program analyzes the images processed (see figure 2.7) by the inversion programs and recreate the energy flux profile.

[1] Convolution of two functions $f*g$ is a particular integral transform: $(f*g) = \int_{-\infty}^{\infty} f(\tau)g(t-\tau)\mathrm{d}\tau$

[2] the low-pass filter used for this program is a Fermi one, defined as $D(j,k) = \frac{1}{1+e^{\frac{\sqrt{k^2+j^2}-\eta}{s}}}$, where s is the filter velocity, set to 1, η is the filter value, j and k are coordinates in the Fourier space[23].

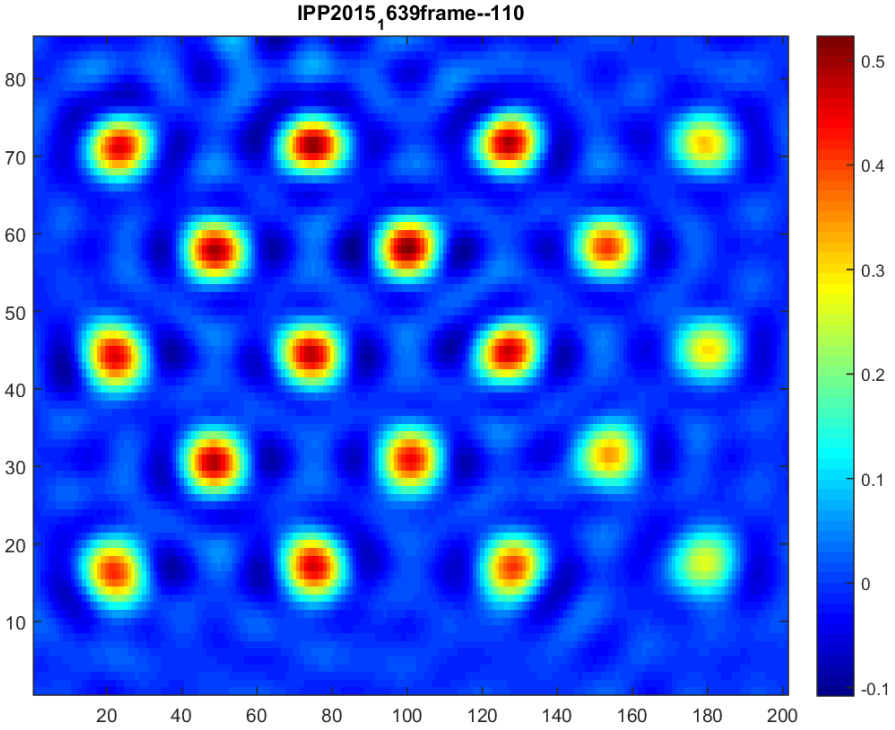

Figure 2.5: Example of a energy flux profile

The fitting function, as already mentioned, is a gaussian function. First the program searches for the single peaks centres positions (see 2.6), with an initial guess of them.

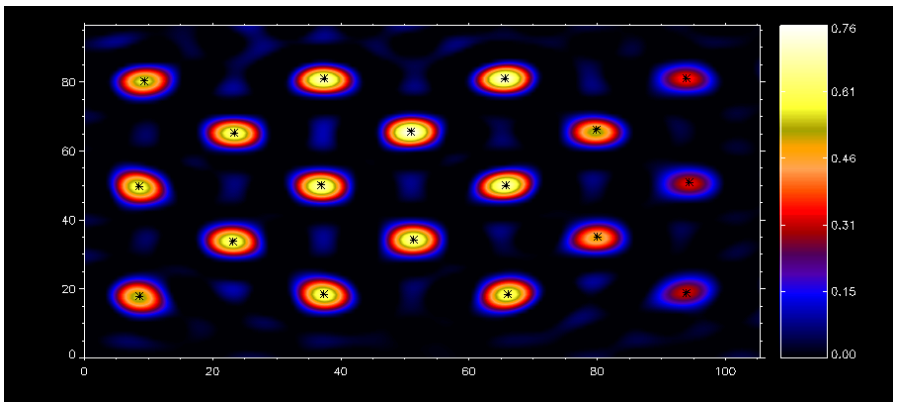

Figure 2.6: Image produced by the fit program after it found the centres of a single tile

To determine the amplitude of the peaks a superposition of 36 Gaussian function is operated.

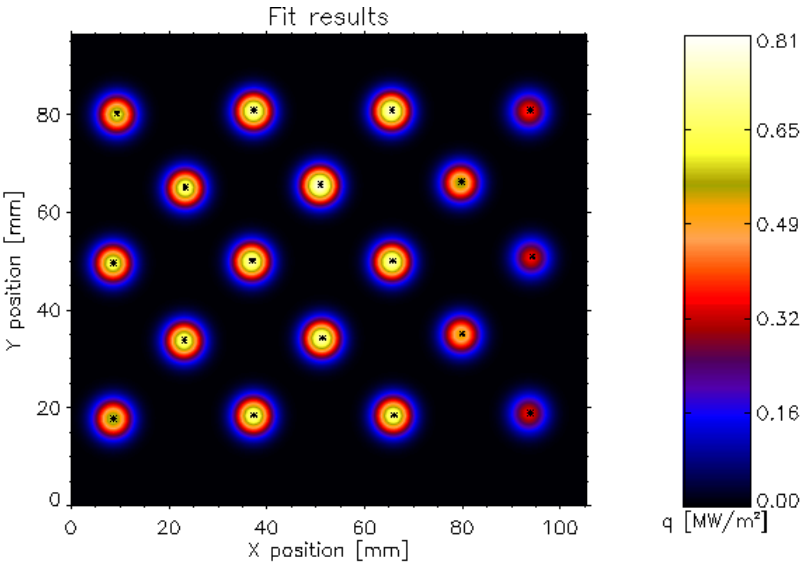

Figure 2.7: An image of the fit of a single tile

The last fit reconstruct the energy flux in front of the copper mask. The vertical profile of this global fit is not symmetrical[22], and so is fitted with a skewed gaussian function:

$$g(x) = \exp\left(\frac{1}{2}\left(\frac{x - x_0}{\omega}\right)^2\right)\left(1 + \operatorname{erf}\left(\alpha\frac{x - x_0}{\sqrt{2}\omega}\right)\right) \tag{2.4}$$

where α is the skewness and the erf is the error function:

$$\operatorname{erf} = \frac{2}{\sqrt{\pi}}\int_0^x e^{-t^2}\mathrm{d}t \tag{2.5}$$

There are three parameters: the peak center x_0, a kind of standard deviation ω and the skewness α. The horizontal profile has a low resolution (5 points), and so it is fitted with a parabola

$$p(y) = ay^2 + by + c \tag{2.6}$$

and so the complete fitting function is

$$f(x, y) = g(x)p(y) \tag{2.7}$$

an example of the fits are on figures 2.8, 2.9, and 2.10.

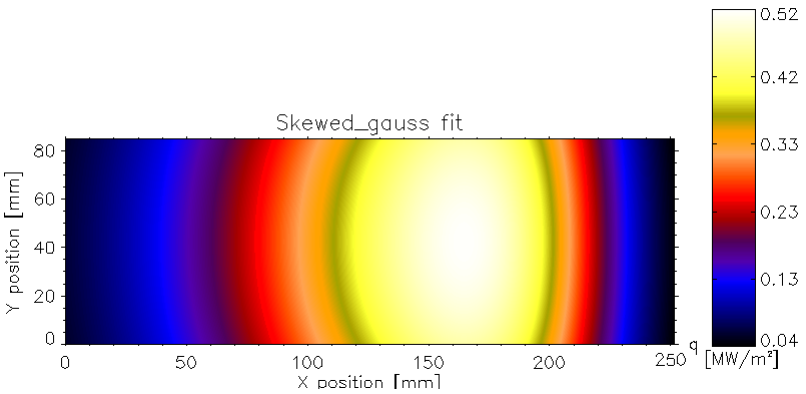

Figure 2.8: Example of a global fit, IPP2014_0389, 90$^{\text{th}}$ frame

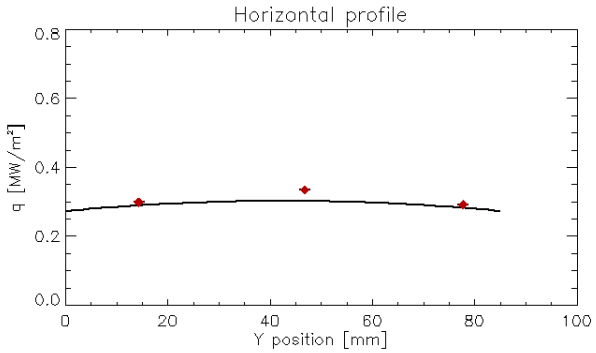

Figure 2.9: Example of a horizontal fit, IPP2014_0389, 90$^{\text{th}}$ frame

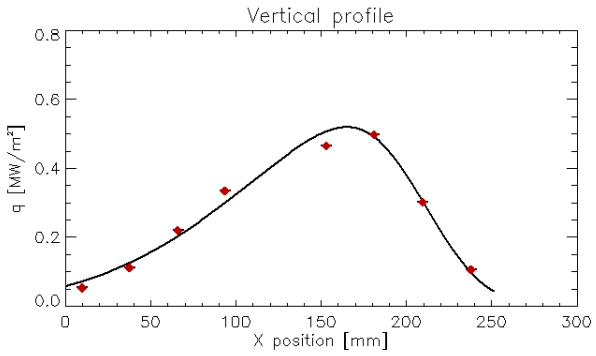

Figure 2.10: Example of a vertical fit, IPP2014_0389, 90$^{\text{th}}$ frame

The fit programs provides as well the values of FWHM, HWHM$_{\text{TOP}}$ and

$HWHM_{BOTTOM}$ of the global fit. The meaning of TOP/BOTTOM differences is explained in figure 2.11. These values, in particular the ratio between HWHMs will be used in data analysis as indicators of the vertical asymmetry of the beam.

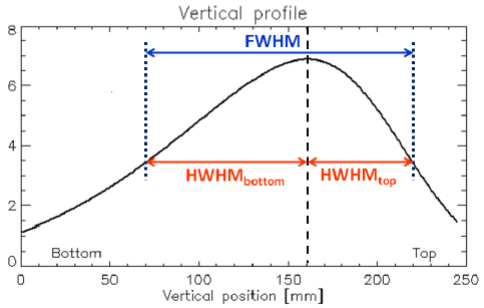

Figure 2.11: The vertical profile of a global fit

Chapter 3

Data Analysis

In this chapter, the procedure to calibrate the inversion program will be explained, as well as the investigations of correlations between source parameters and mini-STRIKE acquired data, studying campaign that has been carried out on BATMAN. The source parameter that can be managed by the NBI operator are:

- the radio-frequency power
- the gas pressure in the ion source
- the acceleration voltage
- the extraction voltage
- the bias voltage

3.1 Filter calibration

In order to study the energy flux optimally the inversion program needs to be calibrated, in particular the value of the low-pass filter. This filter dampens oscillation phenomenon, as already noted in the precedent section 2.1.1. Firstly, a pulse has been analyzed by changing the parameter of the low-pass filter of the inversion from a η (filter cutoff frequency) value of 3.3 to 7.5. The physical quantities that have been studied were the dependence of the value of the filter on HWHM of the gaussian fitting energy flux, the form of the reconstructed temperature profile by the transfer function and the χ^2 of the fit.

3.1.1 Temperature and Energy Flux Comparison

As heat propagates inside the CFC tile, the profile of the temperature is distorted during heat conduction, and even with a CFC tile with strong anisotropy, we can't eliminate this effect.

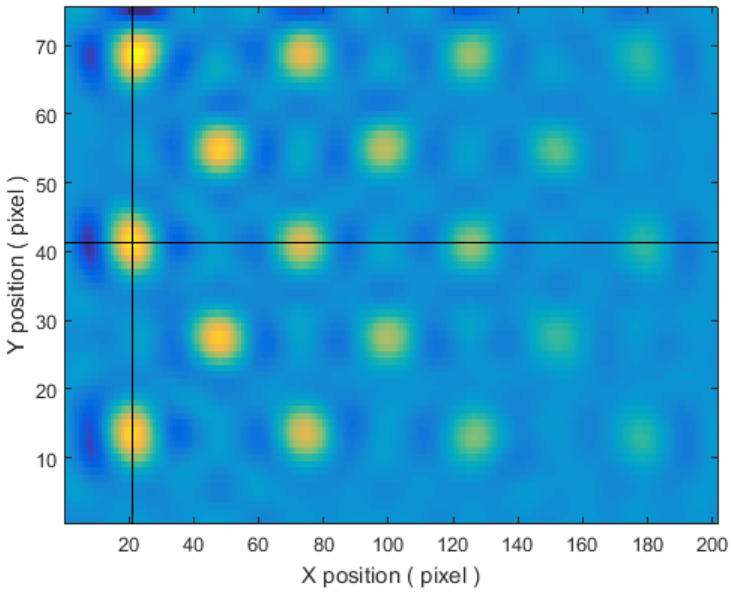

Figure 3.1: Energy flux profile, top tile

The broadening of the profiles can be seen in figure 3.2 (horizontally), and figure 3.3(vertically). These profiles were extracted from the temperature profile and the energy flux profile of the pulse IPP2014_0180 (in figure 3.1 the sampling of the profile is shown on the black line).

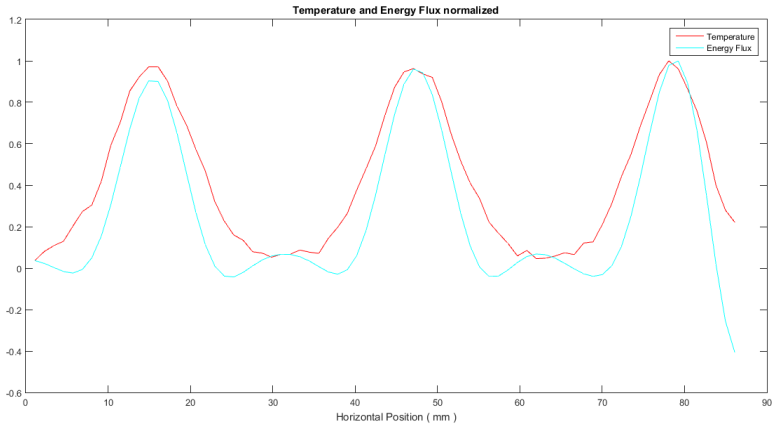

Figure 3.2: Comparison of the two profiles, with a normalization with respect of the height, horizontally

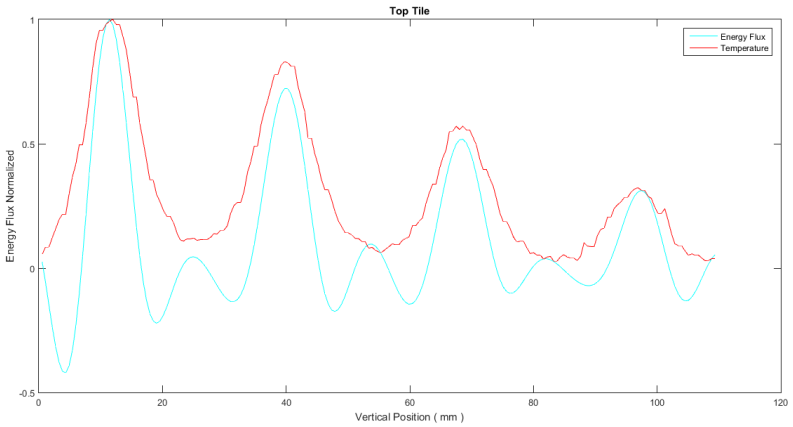

Figure 3.3: Comparison of the two profiles, with a normalization with respect of the height, vertically

3.1.2 Total power

From a operational point of view, the parameter of the NBI does not change over a pulse, so it is expected that the energy flux on the front side of the tile should not change temporally, as the value of the flux is determined by the electric potential of the grid system and by the electric current. However, the inversion program applies various and intrusive process to the data. With this in mind, a small variation of the flux within time of pulses (around 15%, see figure 3.4) was accepted.

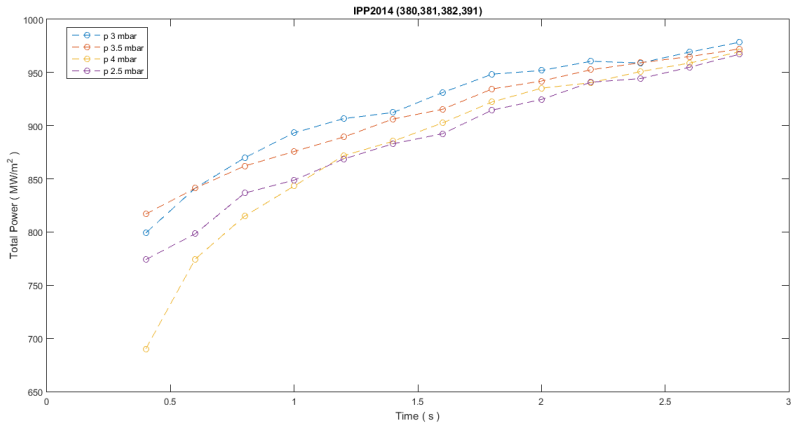

Figure 3.4: Total power as a function of time comparing four pulses of a pressure scan campaign

By changing the η value, total power changes slightly, apart for an isolated

case (3.3) (figure 3.5).

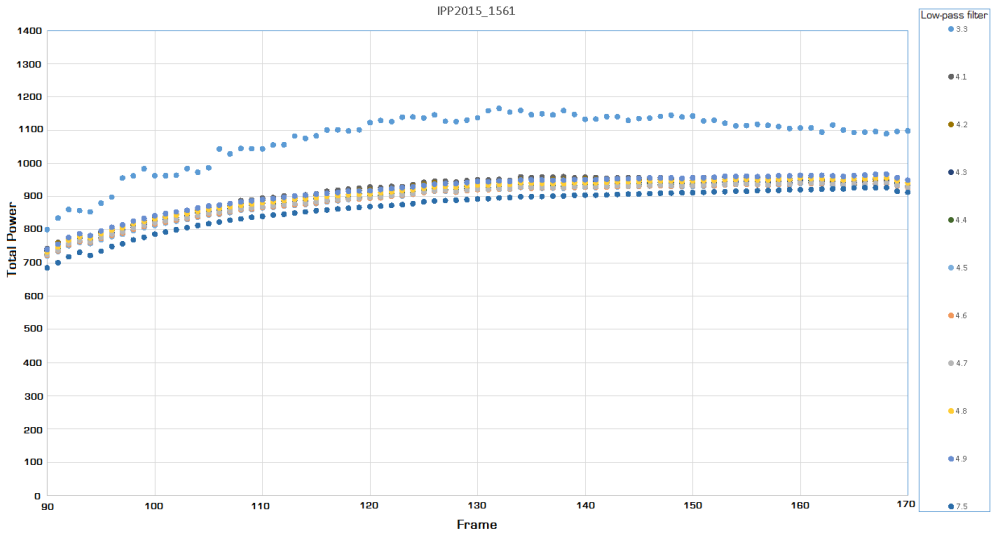

Figure 3.5: Total power as a function of time with several inversions with different η

This validates the inversion program, as flux remains stable within the time interval studied.

3.1.3 Gaussian width

As already described, for the BATMAN experiment a copper mask is placed before the CFC tile, with 18×2 holes of 7 mm of diameters. The inversion program uses gauss functions to approximate a point-like stress (a Dirac δ function approximation) to the CFC tiles of the single beamlets. Additionally, the low-pass filter alters the shape of the function. The value of HWHM (Half Width at Half Maximum[1], $\approx 1.177\sigma$) was studied as a function of time and filter strength. At the beginning of the pulse, the first 10 frames ($\Delta t = 0.4$ s) are discarded from analysis, as in the initial transient the boundary condition of the the inversion model are not respected. As shown in figure 3.6, the value of HWHM remains stable (there is a fluctuation over time, $\approx 15\%$) until 4.6, then it rises linearly.

[1]the HWHM is half of the Full Width at Half Maximum, an expression of the extent of a function given by the difference between the two extremes values of the independent variable at which the dependent variable is equal to half its maximum value

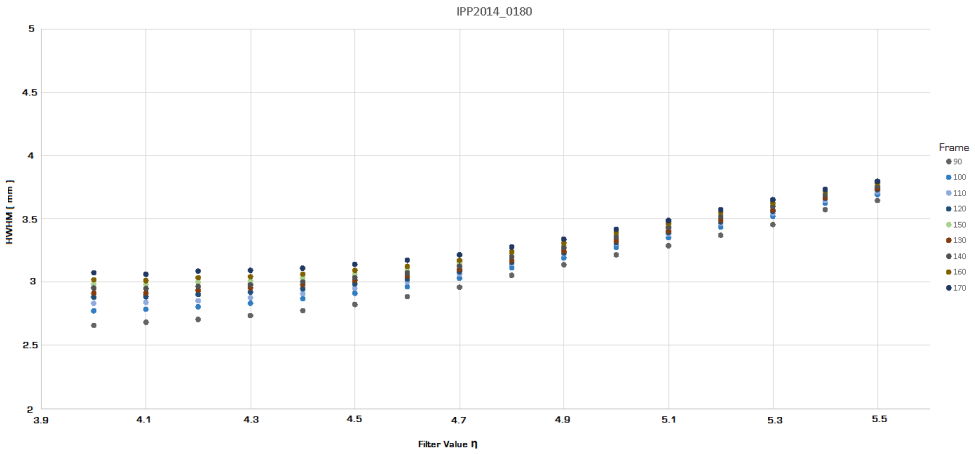

Figure 3.6: HWHM as a function of η, with various frames

and this was expected as the filter smooths the curve. The 76% of the beam power is inside the boundary of the FWHM. Given this information, an upper limit on HWHM was imposed: any pulse with a HWHM value ≥ 3.5 mm would be discarded, as too much power would be distributed outside the hole regions.

3.1.4 Temperature profile reconstruction

The reconstructed energy flux has then been given to COMSOL as input to verify the temperature profile on the backside of the tile, in order to verify the method (see figures 3.7, 3.8).

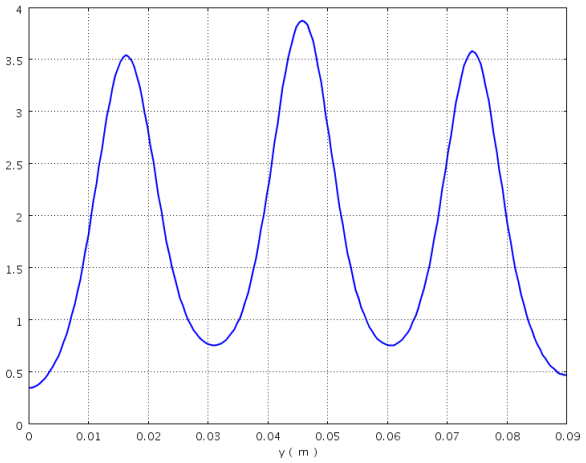

Figure 3.7: Reconstructed horizontal temperature profile, IPP2015_1639 at 1.2 s

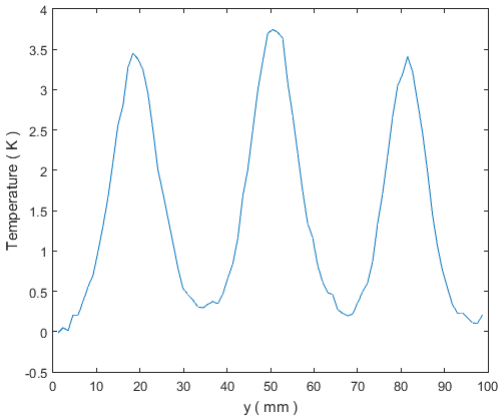

Figure 3.8: Original temperature, IPP2015_1639 at 1.2 s

Between experimental temperature profile and the one processed there is a small fluctuation in the peaks, while the inverted temperature does not return to zero on its edges. This has been deemed acceptable for the analysis.

3.1.5 χ^2 evaluation

Finally, the χ^2 value was studied across η. While there is a small variation of this goodness indicator of the fit, the χ^2 decrease until a "plateau" is found from 4.8 to 5, (see 3.9), then it decreases again. However, further values of the filter were discarded as they had an excessive total power space broadening, as already noted.

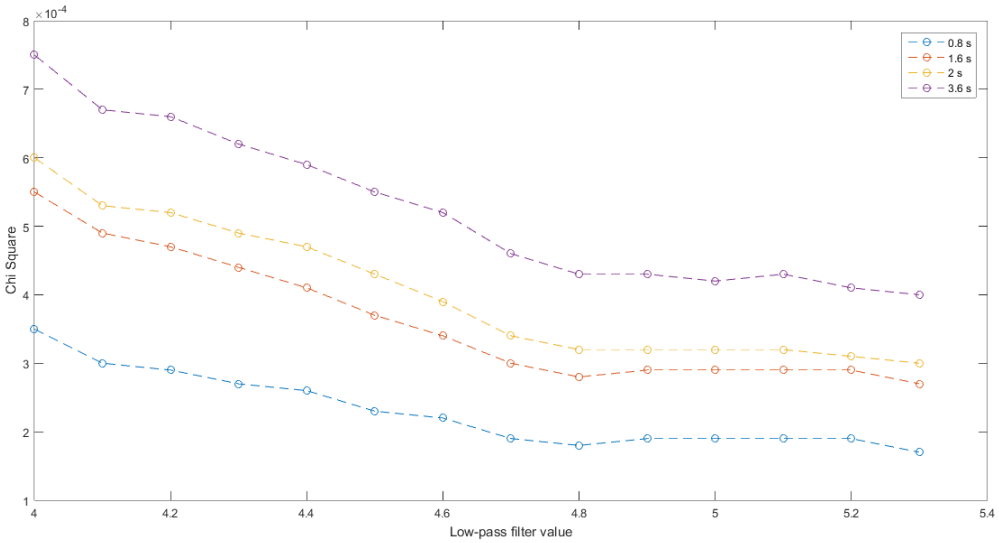

Figure 3.9: χ^2 as a function of the filter, at different times

The values of χ^2 has negligible differences on the plateau. In the case of the value of 4.8 the value of HWHM is inside the 3.5 mm bound until last frames (160 / circa 3.2 s), and more power falls inside the 3.5 mm radius of the holes in comparison with higher values, so it has chosen as the final value for the filter.

3.1.6 Pulse comparison

A series of five pulses has been studied over time, with constant η, to ensure the data behavior was consistent (figure 3.10). Since each pulse has different beam power, each has been normalized in respect with their maximum, enabling comparison within them. The width does not change

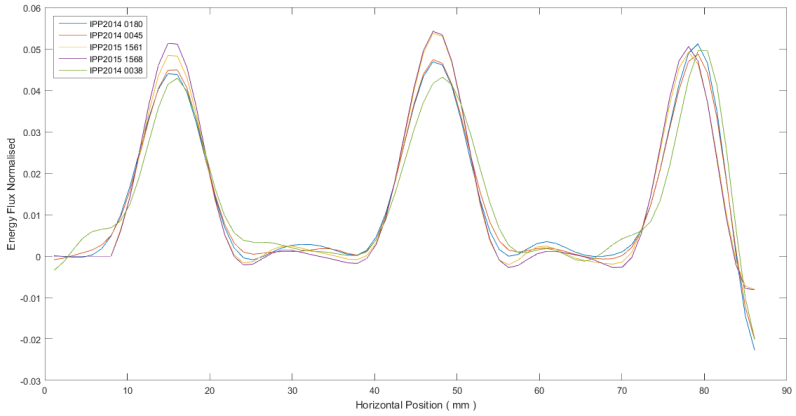

Figure 3.10: The five pulses, with normalized integral for the sake of comparison, horizontal profile

3.2 Parameter scans

This section describe the analysis of some pulses of a experimental campaign. This campaign was conducted by changing a single source parameter while keeping the other constant, like U_{ex}, U_{acc}, pressure inside BATMAN and RF coil power, to study the evolution of acquired data as functions of that variable.

3.2.1 Acceleration Voltage Analysis

In this campaign the only source parameter to change was the acceleration voltage. In table 3.1 the values are shown of the constant parameters. As well as the fit results of the energy flux, some of the most important fit results of the temperature profile will be shown, to compare the two methods of study.

Table 3.1: BATMAN parameters for the acceleration voltage scan

Source pressure (p)	0.5 Pa
Extraction voltage (U_{ex})	5 kV
Plasma drift (tile)	UP
Radio-frequency power (P_{RF})	50 kW
Bias current (I_{bias})	15 A
Hydrogen Isotope	Deuterium

Increasing the U_{acc}, the energy flux of the beam increases as well.

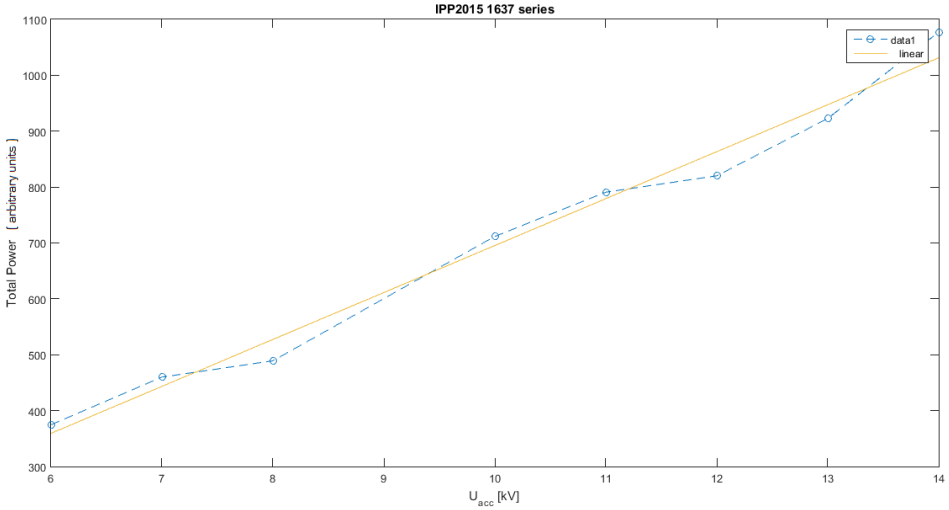

Figure 3.11: Total power as a function of acceleration voltage

In figure 3.11, total power of the energy flux depends on the acceleration potential, as it was expected. A linear fit was calculated to have an approximation of the trend:

$$f(x) = ax + b \tag{3.1}$$

Table 3.2: Fit parameter

a	**b**
83.986	-144.56

The ratio of extraction voltage to acceleration voltage is correlated with the divergence of the beamlets, as already described in section 1.5. In figure 3.12 the normalized perveance is correlated with the FWHM of the global fit.

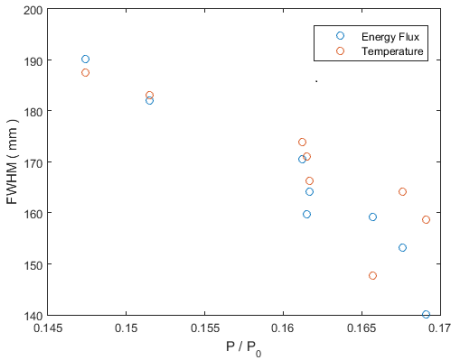

Figure 3.12: FWHM of the global fit as a function normalized perveance

The figure shows a variation of $\approx 16\%$ on the normalized perveance value and $\approx 20\%$ on the voltage ratio. From the figure it appears that the data are collected in underperveant conditions; a similar trend was found in [?, maurizio] Over the acceleration scan, the vertical profile of the same frame is illustrated to show the evolution of the profile with this change (see figure 3.15), and two global profiles to show general trend (figures 3.13, 3.14), acceleration voltage and normalized perveance are noted in table 3.3.

Table 3.3: Campaign Acceleration Voltages and Normalized Perveance

Pulse Name	Acceleration Voltage (kV)	Normalized Perveance
IPP2015_1638	13.35	0.1691
IPP2015_1639	12.27	0.1657
IPP2015_1640	11.34	0.1676
IPP2015_1641	10.24	0.1615
IPP2015_1642	9.32	0.1617
IPP2015_1643	8.34	0.1612
IPP2015_1644	7.2	0.1515
IPP2015_1645	6.21	0.1474

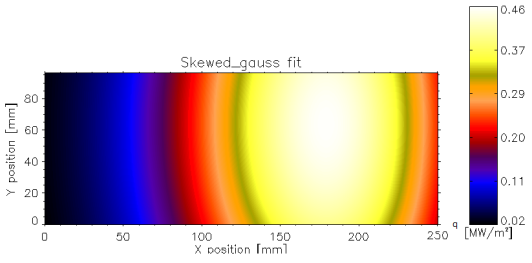

Figure 3.13: Profile of the fitting function for IPP2015_1640

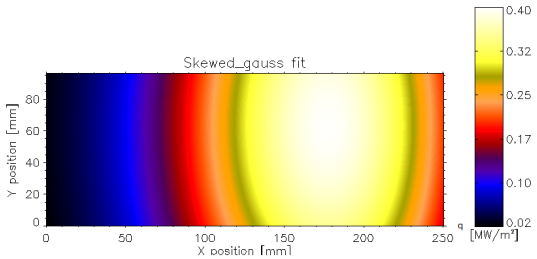

Figure 3.14: Profile of the fitting function for IPP2015_1641

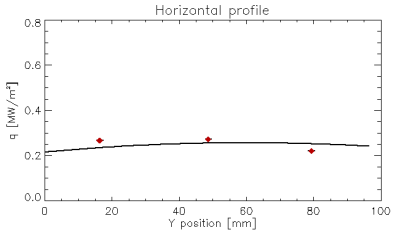

(a) Horizontal profile of the fitting function for IPP2015_1638

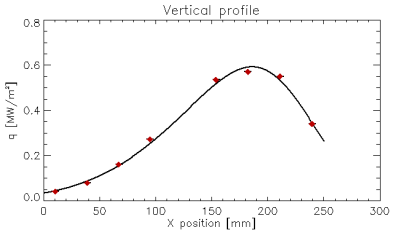

(b) Vertical profile of the fitting function for IPP2015_1638

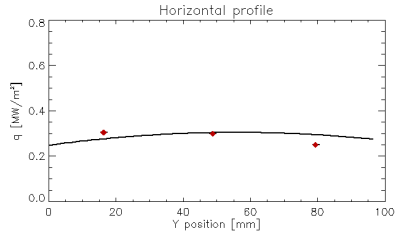

(c) Horizontal profile of the fitting function for IPP2015_1637

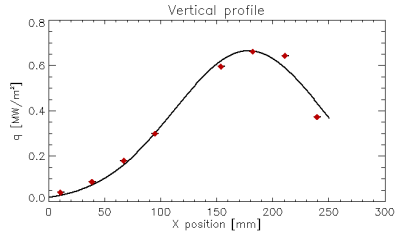

(d) Vertical profile of the fitting function for IPP2015_1637

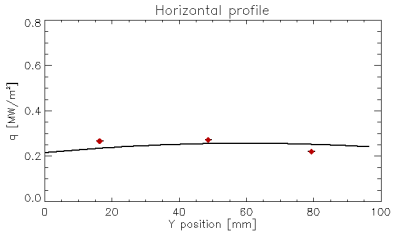

(e) Horizontal profile of the fitting function for IPP2015_1638

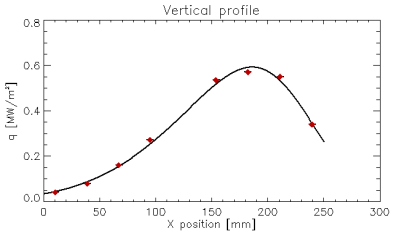

(f) Vertical profile of the fitting function for IPP2015_1638

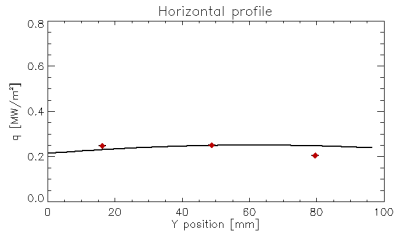

(g) Horizontal profile of the fitting function for IPP2015_1639

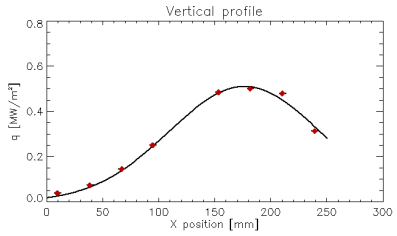

(h) Vertical profile of the fitting function for IPP2015_1639

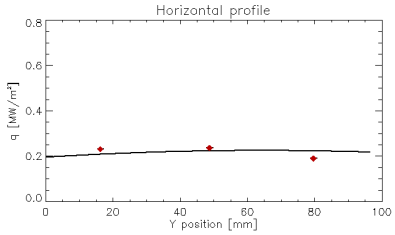

(i) Horizontal profile of the fitting function for IPP2015_1640

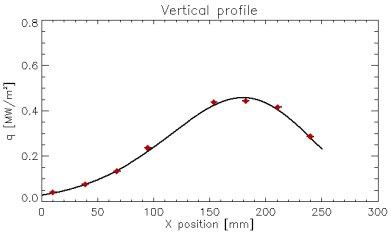

(j) Vertical profile of the fitting function for IPP2015_1640

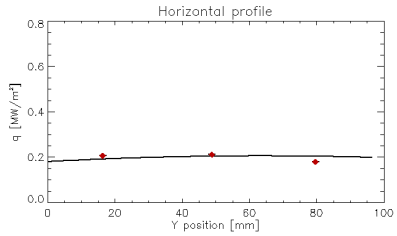

(k) Horizontal profile of the fitting function for IPP2015_1641

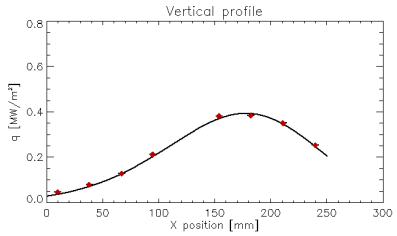

(l) Vertical profile of the fitting function for IPP2015_1641

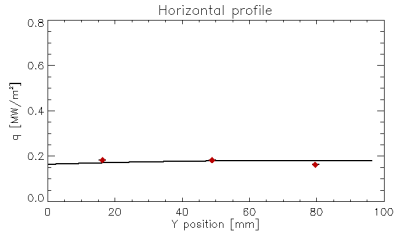

(m) Horizontal profile of the fitting function for IPP2015_1642

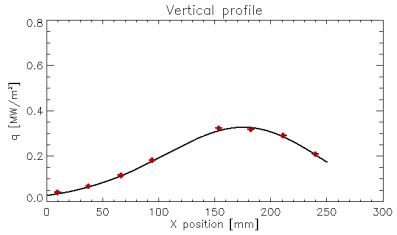

(n) Vertical profile of the fitting function for IPP2015_1642

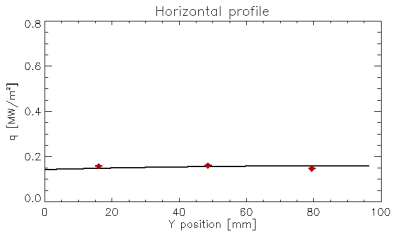

(o) Horizontal profile of the fitting function for IPP2015_1643

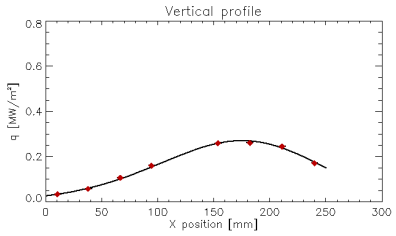

(p) Vertical profile of the fitting function for IPP2015_1643

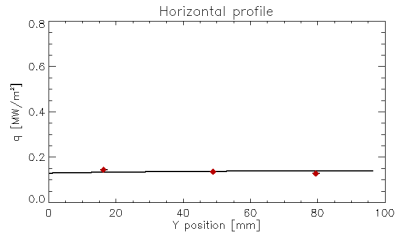

(q) Horizontal profile of the fitting function for IPP2015_1644

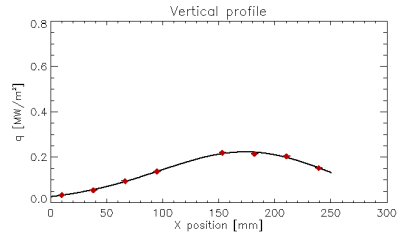

(r) Vertical profile of the fitting function for IPP2015_1644

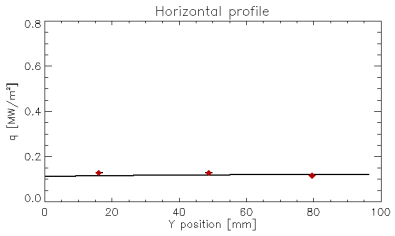

(s) Horizontal profile of the fitting function for IPP2015_1645

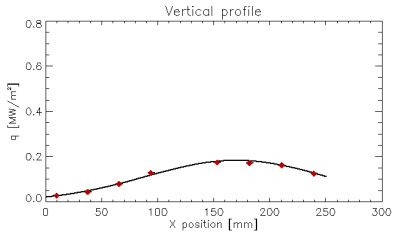

(t) Vertical profile of the fitting function for IPP2015_1645

Figure 3.15: Profiles of the functions for the acceleration voltage scan

While the horizontal profile trend is slightly affected by voltage acceleration parameter, the vertical profile is decreasing, furthermore the shape of the vertical profile is smoothed. This effect is better shown in figure 3.16, where the ratio of $HWHM_{TOP}$ to $HWHM_{BOTTOM}$ is correlated with the ratio of extraction voltage to acceleration voltage. The skewed gauss function slowly becomes less skewed as the ratio between the voltages increases. A ratio of 1 in the case of HWHMs ratio means that the function is symmetrical.

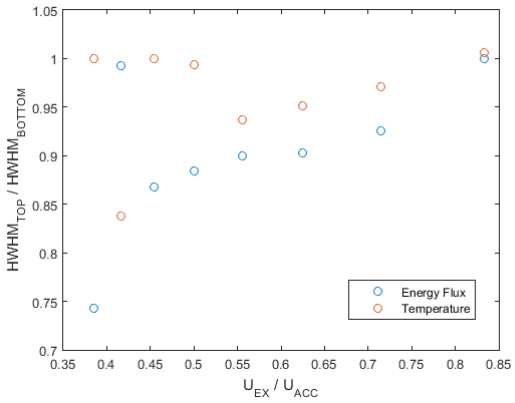

Figure 3.16: The ratios of HWHMs as a function of the ratio of the extraction voltage to acceleration voltage

The position of the peak centre shifts towards the intersection of the tiles while the acceleration voltage decreases (see 3.17).

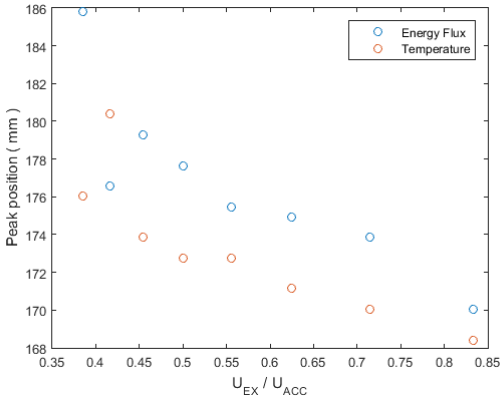

Figure 3.17: The shifting vertical maximum is shown as a function of the voltage ratio

The FWHM increases as the voltage ratio increases (figure 3.18). This can be seen in the precedent profile figures, as the energy flux of the beam decreases, the function is broadening.

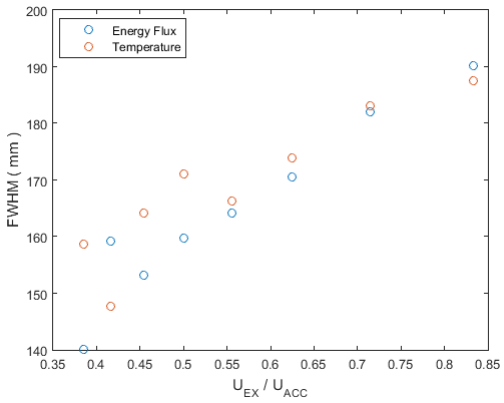

Figure 3.18: FWHM in function of the voltage ratio

Chapter 4

Conclusions

ITER is the collective effort of several nations to build a thermonuclear reactor with an energy output bigger than the energy required to operate it, a result still not yielded by any fusion reactor. ITER needs plasma heating to reach the necessary temperature for nuclear fusion. One of the methods that will be used is injection of neutral beam inside the reactor, using a negative ion source. Various test facility have been built to investigate the properties of the source and the beam, and to optimize the diagnostics and to study neutral beam behavior. SPIDER is the ion source under construction at Padova that will accelerate the beam at 100 keV, and one of the main diagnostics will be STRIKE, a calorimeter whose main components are 16 uni-directional carbon fibre composite carbon (CFC) tiles, on which the beam will impinge. An IR camera will acquire thermal profile on the back side of the tiles.
BATMAN (BAverian Test MAchine for Negative ions), at Max-Planck Institut für Plasmaphysik, in IPP-Garching bei München in Germany, is the one of the prototype of the RF ion source for ITER, in which its main measurements device is the calorimeter mini-STRIKE, a smaller version of STRIKE, was used for test of the diagnostic and to characterize the BATMAN beam.

4.1 Thesis work

The goals of the mini-STRIKE are to characterize the neutral beam of the BATMAN experiments. To this purpose, a method was realized to reconstruct the beam energy flux profile from the two-dimensional pattern of the measured temperature. One of the main activities of this thesis work was to calibrate the cutoff frequency of the Fermi filter in order to optimizing the reconstruction of the energy flux of the neutral beam impinging on the CFC tile, as well as to apply the reconstruction method to an experimental campaign. The thesis offers a framework that can be used for future calibrations on the next experiments that will use STRIKE calorimeter.
In the section "Filter Calibration" it has been shown how the optimal cutoff frequency value is 4.8, using several parameters, such as χ^2, HWHM, stability of energy flux over time, *etc.* In the subsequent section, a campaign scan over acceleration voltage was analyzed as a test bench for the chosen filter value. Results were inside expected parameter behavior: an increases in acceleration

voltage produced an increase in the total power of the flux, as well as a reduction of the beamlet divergence, *etc.*.

4.2 Future research

The inversion method has been extensively tested to ensure the calibration was optimal, and that it would function across various campaigns and pulses of BATMAN. As a future work, the method needs to be applied to all campaigns to study the various correlations between the ion source parameter.

Bibliography

[1] G. Brumfiel, *Fusion dreams delayed*, Nature, **459**, pp. 488-489, 27 May 2009.

[2] *Fusion Physics*, International Atomic Energy Agency, Vienna, 2012.

[3] J.P. Freidberg, *Plasma physics and fusion energy*, Cambridge University Press, 2007.

[4] V.P. Smirnov, *Tokamak foundation in USSR/Russia 1950–1990*, IOP Publishing and Internation Atomic Energy Agency, vol. **50**, pp. 1-2, 30 December 2009.

[5] Solovev, L. S. and Shafranov, V. D., *Review of Plasma Physics*, Vol. 5, pp. 1, New York, 1966.

[6] https://www.euro-fusion.org/

[7] M G Haines, *The Joule Heating of a Stable Pinched Plasma*, Proceedings of the Physical Society, vol. 76, no. 2, 1960.

[8] Ronald Stephen Hemsworth and Takashi Inoue, *Positive and Negative Ion Sources for Magnetic Fusion*, IEEE Transactions on Plasma Science, **33**, 1799-1813, 2005.

[9] R. Behrisch, *Sputtering by Particle bombardment*, Springer, Berlin, 1981.

[10] A. Rizzolo et al., *Fusion Eng. Des.*, **85**, 2268, 2010.

[11] G. Serianni, M. De Muri, A. Rizzolo *et al.*, *First negative ion beam measurement by the Short-Time Retractable Instrumented Kalorimeter Experiment (STRIKE)*, Review of Scientific Instruments, **85**, 14 January 2014.

[12] V. Cervaro, S. Cristofaro, S. Dal Bello, M. Dalla Palma, M. De Muri, D: Fasolo, L. Franchin, A. Muraro, R. Pasqualotto, A: Rizzolo, G. Serianni, M. Tollin, *Characterisation of STRIKE tiles by laser pulses*, Consorzio RFX, pp 29, 2013.

[13] A.W. Chao and M. Tigner, *Handbook of Accelerator Physics and Engineering*, World Scientific, p. 100, 1999.

[14] P. Sonato, P. Agostinetti, G. Serianni *et al.*, *The ITER full size plasma source device design*, Fusion Engineering and Design, vol. 84, pp. 269–274, 2009.

[15] I. Langmuir, *The effect of space charge and residual gases on thermionic currents in high vacuum*, Phys. Rev. vol 2, pp 450, 1913.

[16] Kittel, Charles, *Introduction to Solid State Physics (7th ed.)*, Wiley.

[17] Y. Okumura, M. Hanada, T. Inoue, H. Kojima, Y. Matsuda, Y. Ohara, M. Seki, and K.Watanabe, *Cesium mixing in the multi-ampere volume H^- ion source*, in *Proc. 5th Int. Symp. Production Neutralization Negative Ions Beams*, Upton, NY, AIP Conf. Proc. 40, pp. 169–183 1990.

[18] D. Riz and J. Paméla, *Modeling of negative ion transport in a plasma source*, Rev. Sci. Instrum., vol. 69, no. 2, pp. 914–919, Feb. 1998.

[19] G. Serianni, M. De Muri,A. Muraro, P. Veltri, F. Bonomo, G. Chitarin, R. Pasqualotto, M. Pavei, A. Rizzolo, M. Valente, P. Franzen, B. Ruf, L. Schiesko, *First negative ion beam measurement by the Short-Time Retractable Instrumented Kalorimeter Experiment (STRIKE)*, Review of Scientific Instruments, **85**, 2014.

[20] A. Rizzolo et al., Fusion Engineering and Design, vol. 85, 2010.

[21] R. S. Delogu, C. Poggi, A. Pimazzoni, G. Rossi, G. Serianni, *Analysis of diagnostic calorimeter data by the transfer function technique*, Rev. Sci. Instrum., **87** 2016.

[22] S. Cristofaro, *Characterisation of the BATMAN beam properties by H_α-Doppler shift spectroscopy and mini-STRIKE calorimeter*, Master Thesis, University of Padova, pp. 51, 2014.

[23] C. Poggi, *Analisi dei dati del calorimetro STRIKE utilizzando la tecnica della funzione di trasferimento*, Undergrad Thesis, University of Padova, pp. 40, 2015.

[24] R. Maurizio, *Beam property characterization by means of three beam diagnostics at BATMAN*, Master Thesis in Physics, University of Padova, 2015.